Superconducting Qubits: A Short Review

M. H. Devoret[†], A. Wallraff[†], and J. M. Martinis[*]

[†]Department of Applied Physics, Yale University, New Haven, CT 06520
[*]Department of Physics, University of California, Santa Barbara, CA 93106

November 26, 2024

Abstract

Superconducting qubits are solid state electrical circuits fabricated using techniques borrowed from conventional integrated circuits. They are based on the Josephson tunnel junction, the only non-dissipative, strongly non-linear circuit element available at low temperature. In contrast to microscopic entities such as spins or atoms, they tend to be well coupled to other circuits, which make them appealing from the point of view of readout and gate implementation. Very recently, new designs of superconducting qubits based on multi-junction circuits have solved the problem of isolation from unwanted extrinsic electromagnetic perturbations. We discuss in this review how qubit decoherence is affected by the intrinsic noise of the junction and what can be done to improve it.

Contents

1 Introduction

1.1 The problem of implementing a quantum computer

The theory of information has been revolutionized by the discovery that quantum algorithms can run exponentially faster than their classical counterparts, and by the invention of quantum error-correction protocols [1]. These fundamental breakthroughs have lead scientists and engineers to imagine building entirely novel types of information processors. However, the construction of a computer exploiting quantum – rather than classical – principles represents a formidable scientific and technological challenge. While quantum bits must be strongly inter-coupled by gates to perform quantum computation, they must at the same time be completely decoupled from external influences, except during the write, control and readout phases when information must flow freely in and out of the machine. This difficulty does not exist for the classical bits of an ordinary computer, which each follow strongly irreversible dynamics that damp the noise of the environment.

Most proposals for implementing a quantum computer have been based on qubits constructed from microscopic degrees of freedom: spin of either electrons or nuclei, transition dipoles of either atoms or ions in vacuum. These degrees of freedom are naturally very well isolated from their environment, and hence decohere very slowly. The main challenge of these implementations is enhancing the inter-qubit coupling to the level required for fast gate operations without introducing decoherence from parasitic environmental modes and noise.

In this review, we will discuss a radically different experimental approach based on "quantum integrated circuits." Here, qubits are constructed from *collective* electrodynamic modes of macroscopic electrical elements, rather than microscopic degrees of freedom. An advantage of this approach is that these qubits have intrinsically large electromagnetic cross-sections, which implies they may be easily coupled together in complex topologies via simple linear electrical elements like capacitors, inductors, and transmission lines. However, strong coupling also presents a related challenge: is it possible to isolate these electrodynamic qubits from ambient parasitic noise while retaining efficient communication channels for the write, control, and read operations? The main purpose of this article is to review the considerable progress that has been made in the past few years towards this goal, and to explain how new ideas about methodology and materials are likely to improve coherence to the threshold needed for quantum error correction.

1.2 Caveats

Before starting our discussion, we must warn the reader that this review is atypical in that it is neither historical nor exhaustive. Some important works have not been included or are only partially covered. We amply cite work by our own, at the risk of irritating the reader, but we wanted to base our speculations on experiments whose details we fully understand. We have on

purpose narrowed our focus: we adopt the point of view of an engineer trying to determine the best strategy for building a reliable machine given certain design criteria. This approach obviously runs the risk of presenting a biased and even incorrect account of recent scientific results, since the optimization of a complex system is always an intricate process with both hidden passageways and dead-ends. We hope nevertheless that the following sections will at least stimulate discussions on how to harness the physics of quantum integrated circuits into a mature quantum information processing technology.

2 Basic features of quantum integrated circuits

2.1 Ultra-low dissipation: superconductivity

For an integrated circuit to behave quantum mechanically, the first requirement is the absence of dissipation. More specifically, all metallic parts need to be made out of a material that has zero resistance at the qubit operating temperature and at the qubit transition frequency. This is essential in order for electronic signals to be carried from one part of the chip to another without energy loss – a necessary (but not sufficient) condition for the preservation of quantum coherence. Low temperature superconductors such as aluminium or niobium are ideal for this task [2]. For this reason, quantum integrated circuit implementations have been nicknamed "superconducting qubits"[1].

2.2 Ultra-low noise: low temperature

The degrees of freedom of the quantum integrated circuit must be cooled to temperatures where the typical energy kT of thermal fluctuations is much less that the energy quantum $\hbar\omega_{01}$ associated with the transition between the states $|qubit = 0\rangle$ and $|qubit = 1\rangle$. For reasons which will become clear in subsequent sections, this frequency for superconducting qubits is in the 5-20 GHz range and therefore, the operating temperature temperature T must be around 20 mK (Recall that 1 K corresponds to about 20 GHz). These temperatures may be readily obtained by cooling the chip with a dilution refrigerator. Perhaps more importantly though, the "electromagnetic temperature" of the wires of the control and readout ports connected to the chip must also be cooled to these low temperatures, which requires careful electromagnetic filtering. Note that electromagnetic damping mechanisms are usually stronger at low temperatures than those originating from electron-phonon coupling. The techniques [3] and requirements [4] for ultra-low noise filtering have been known for about 20 years. From the requirements $kT \ll \hbar\omega_{01}$ and $\hbar\omega_{01} \ll \Delta$, where Δ is the energy gap

---

[1]In principle, other condensed phases of electrons, such as high-Tc superconductivity or the quantum Hall effect, both integer and fractional, are possible and would also lead to quantum integrated circuits of the general type discussed here. We do not pursue this subject further than this note, however, because dissipation in these new phases is, by far, not as well understood as in low-Tc superconductivity.

of the superconducting material, one must use superconducting materials with a transition temperature greater than about 1K.

2.3 Non-linear, non-dissipative elements: tunnel junctions

Quantum signal processing cannot be performed using only purely linear components. In quantum circuits, however, the non-linear elements must obey the additional requirement of being non-dissipative. Elements like PIN diodes or CMOS transistors are thus forbidden, even if they could be operated at ultra-low temperatures.

There is only one electronic element that is both non-linear and non-dissipative at arbitrarily low temperature: the superconducting tunnel junction[2] (also known as a Josephson tunnel junction [5]). As illustrated in Fig. 1, this circuit element consists of a sandwich of two superconducting thin films separated by an insulating layer that is thin enough (typically $\sim$1 nm) to allow tunneling of discrete charges through the barrier. In later sections we will describe how the tunneling of Cooper pairs creates an inductive path with strong non-linearity, thus creating energy levels suitable for a qubit. The tunnel barrier is typically fabricated from oxidation of the superconducting metal. This results in a reliable barrier since the oxidation process is self-terminating [7]. The materials properties of amorphous aluminum oxide, alumina, make it an attractive tunnel insulating layer. In part because of its well-behaved oxide, aluminum is the material from which good quality tunnel junctions are most easily fabricated, and it is often said that aluminium is to superconducting quantum circuits what silicon is to conventional MOSFET circuits. Although the Josephson effect is a subtle physical effect involving a combination of tunneling and superconductivity, the junction fabrication process is relatively straightforward.

2.4 Design and fabrication of quantum integrated circuits

Superconducting junctions and wires are fabricated using techniques borrowed from conventional integrated circuits[3]. Quantum circuits are typically made on silicon wafers using optical or electron-beam lithography and thin film deposition. They present themselves as a set of micron-size or sub-micron-size circuit elements (tunnel junctions, capacitors, and inductors) connected by wires or transmission lines. The size of the chip and elements are such that, to a large extent, the electrodynamics of the circuit can be analyzed using simple transmission line equations or even a lumped element approximation. Contact to the chip is made by wires bonded to mm-size metallic pads. The circuit can be designed using conventional layout and classical simulation programs.

---

[2]A very short superconducting weak link (see for instance Ref. [6]) is a also a possible candidate, provided the Andreev levels would be sufficiently separated. Since we have too few experimental evidence for quantum effects involving this device, we do not discuss this otherwise important matter further.

[3]It is worth mentioning that chips with tens of thousands of junctions have been successfully fabricated for the voltage standard and for the Josephson signal processors, which are only exploiting the speed of Josephson elements, not their quantum properties.
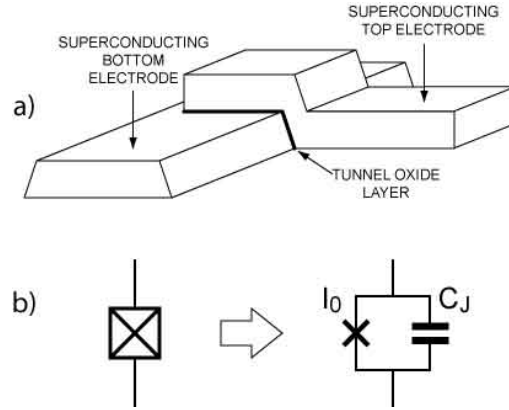
Figure 1: a) Josephson tunnel junction made with two superconducting thin films; b) Schematic representation of a Josephson tunnel junction. The irreducible Josephson element is represented by a cross.

Thus, many of the design concepts and tools of conventional semiconductor electronics can be directly applied to quantum circuits. Nevertheless, there are still important differences between conventional and quantum circuits at the conceptual level.

2.5 Integrated circuits that obey macroscopic quantum mechanics

At the conceptual level, conventional and quantum circuits differ in that, in the former, the collective electronic degrees of freedom such as currents and voltages are classical variables, whereas in the latter, these degrees of freedom must be treated by quantum operators which do not necessarily commute. A more concrete way of presenting this rather abstract difference is to say that a typical electrical quantity, such as the charge on the plates of a capacitor, can be thought of as a simple number in conventional circuits, whereas in quantum circuits, the charge on the capacitor must be represented by a wave function giving the probability amplitude of all charge configurations. For example, the charge on the capacitor can be in a superposition of states where the charge is both positive and negative at the same time. Similarly the current in a loop might be flowing in two opposite directions at the same time. These situations have originally been nicknamed "macroscopic quantum coherence"effects by Tony Leggett [8] to emphasize that quantum integrated circuits are displaying phenomena involving the collective behavior of many particles, which are in contrast to the usual quantum effects associated with microscopic particles such as electrons, nuclei or molecules[4].

---

[4]These microscopic effects determine also the properties of materials, and explain phenomena such as superconductivity and the Josephson effect itself. Both classical and quantum

2.6 DiVincenzo criteria

We conclude this section by briefly mentioning how quantum integrated circuits satisfy the so-called DiVicenzo criteria for the implementation of quantum computation [9]. The non-linearity of tunnel junctions is the key property ensuring that non-equidistant level subsystems can be implemented (criterion # 1: qubit existence). As in many other implementations, initialization is made possible (criterion #2: qubit reset) by the use of low temperature. Absence of dissipation in superconductors is one of the key factors in the quantum coherence of the system (criterion # 3: qubit coherence). Finally, gate operation and read-out (criteria #4 and #5) are easily implemented here since electrical signals confined to and traveling along wires constitute very efficient coupling methods.

3 The simplest quantum circuit

3.1 Quantum LC oscillator

We consider first the simplest example of a quantum integrated circuit, the LC oscillator. This circuit is shown in Fig. 2, and consists of an inductor L connected to a capacitor C, all metallic parts being superconducting. This simple circuit is the lumped-element version of a superconducting cavity or a transmission line resonator (for instance, the link between cavity resonators and LC circuits is elegantly discussed by Feynman [10]). The equations of motion of the LC circuit are those of an harmonic oscillator. It is convenient to take the position coordinate as being the flux Φ in the inductor, while the role of conjugate momentum is played by the charge Q on the capacitor playing the role of its conjugate momentum. The variables Φ and Q have to be treated as canonically conjugate quantum operators that obey $[\Phi, Q] = i\hbar$. The hamiltonian of the circuit is $H = \Phi^2/2L + Q^2/2C$, which can be equivalently written as $H = \hbar\omega_0(n + 1/2)$ where n is the number operator for photons in the resonator and $\omega_0 = 1/\sqrt{LC}$ is the resonance frequency of the oscillator. It is important to note that the parameters of the circuit hamiltonian are not fundamental constants of Nature. They are engineered quantities with a large range of possible values which can be modified easily by changing the dimensions of elements, a standard lithography operation. It is in this sense, in our opinion, that the system is unambiguously "macroscopic". The other important combination of the parameters L and C is the characteristic impedance $Z = \sqrt{L/C}$ of the circuit. When we combine this impedance with the residual resistance of the circuit and/or its radiation losses, both of which we can lump into a resistance R, we obtain the quality factor of the oscillation: $\mathcal{Q} = R/Z$. The theory of the harmonic oscillator shows that a quantum superposition of ground state and first excited state decays on a time scale given by $1/RC$. This last equality illustrates the general link between a classical measure of dissipation and the upper limit of the quantum coherence time.

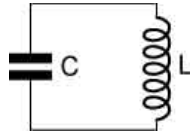circuits share this bottom layer of microscopic quantum mechanics.

Figure 2: Lumped element model for an electromagnetic resonator: LC oscillator.

3.2 Practical considerations

In practice, the circuit shown in Fig. 2 may be fabricated using planar components with lateral dimensions around 10 μm, giving values of L and C approximately 0.1 nH and 1 pF, respectively, and yielding $\omega_0/2\pi \simeq 16$GHz and $Z_0 = 10\,\Omega$. If we use aluminium, a good BCS superconductor with transition temperature of 1.1 K and a gap $\Delta/e \simeq 200\ \mu V$, dissipation from the breaking of Cooper pairs will begin at frequencies greater than $2\Delta/h \simeq 100$GHz. The residual resistivity of a BCS superconductor decreases exponentially with the inverse of temperature and linearly with frequency, as shown by the Mattis-Bardeen (MB) formula $\rho(\omega) \sim \rho_0 \hbar\omega/(k_B T) \exp(-\Delta/k_B T)$ [11], where ρ_0 is the resistivity of the metal in the normal state (we are treating here the case of the so-called "dirty" superconductor [12], which is well adapted to thin film systems). According to MB, the intrinsic losses of the superconductor at the temperature and frequency (typically 20 mK and 20 GHz) associated with qubit dynamics can be safely neglected. However, we must warn the reader that the intrisinsic losses in the superconducting material do not exhaust, by far, sources of dissipation, even if very high quality factors have been demonstrated in superconducting cavity experiments [13].

3.3 Matching to the vacuum impedance: a useful feature, not a bug

Although the intrisinsic dissipation of superconducting circuits can be made very small, losses are in general governed by the coupling of the circuit with the electromagnetic environment that is present in the forms of write, control and readout lines. These lines (which we also refer to as ports) have a characteristic propagation impedance $Z_c \simeq 50\Omega$, which is constrained to be a fraction of the impedance of the vacuum $Z_{\text{vac}} = 377\Omega$. It is thus easy to see that our LC circuit, with a characteristic impedance of $Z_0 = 10\Omega$, tends to be rather well impedance-matched to any pair of leads. This circumstance occurs very frequently in circuits, and almost never in microscopic systems such as atoms which interact very weakly with electromagnetic radiation[5]. Matching to Z_{vac} is a useful feature because it allows strong coupling for writing, reading, and

---

[5]The impedance of an atom can be crudely seen as being given by the impedance quantum $R_K = h/e^2$. We live in a universe where the ratio $Z_{vac}/2R_K$, also known as the fine structure constant $1/137.0$, is a small number.

logic operations. As we mentioned earlier, the challenge with quantum circuits is to isolate them from parasitic degrees of freedom. **The major task of this review is to explain how this has been achieved so far and what level of isolation is attainable.**

3.4 The consequences of being macroscopic

While our example shows that quantum circuits can be mass-produced by standard microfabrication techniques and that their parameters can be easily engineered to reach some optimal condition, it also points out evident drawbacks of being "macroscopic" for qubits.

The engineered quantities L and C can be written as

$$
\begin{aligned}
L &= L^{\mathrm{stat}} + \Delta L\left(t\right) \\
C &= C^{\mathrm{stat}} + \Delta C\left(t\right)
\end{aligned}
\tag{1}
$$

a) The first term on the right-handside denotes the static part of the parameter. It has **statistical variations**: unlike atoms whose transition frequencies in isolation are so reproducible that they are the basis of atomic clocks, circuits will always be subject to parameter variations from one fabrication batch to another. Thus prior to any operation using the circuit, the transition frequencies and coupling strength will have to be determined by "diagnostic" sequences and then taken into account in the algorithms.

b) The second term on the right-handside denotes the time-dependent fluctuations of the parameter. It describes **noise** due to residual material defects moving in the material of the substrate or in the material of the circuit elements themselves. This noise can affect for instance the dielectric constant of a capacitor. The low frequency components of the noise will make the resonance frequency wobble and contribute to the dephasing of the oscillation. Furthermore, the frequency component of the noise at the transition frequency of the resonator will induce transitions between states and will therefore contribute to the energy relaxation.

Let us stress that statistical variations and noise are not problems affecting superconducting qubit parameters only. For instance when several atoms or ions are put together in microcavities for gate operation, patch potential effects will lead to expressions similar in form to Eq. (1) for the parameters of the hamiltonian, even if the isolated single qubit parameters are fluctuation-free.

3.5 The need for non-linear elements

Not all aspects of quantum information processing using quantum integrated circuits can be discussed within the framework of the LC circuit, however. It lacks an important ingredient: non-linearity. In the harmonic oscillator, all transitions between neighbouring states are degenerate as a result of the parabolic

shape of the potential. In order to have a qubit, the transition frequency between states $|\text{qubit} = 0\rangle$ and $|\text{qubit} = 1\rangle$ must be sufficiently different from the transition between higher-lying eigenstates, in particular 1 and 2. Indeed, the maximum number of 1-qubit operations that can be performed coherently scales as $\mathcal{Q}_{01} |\omega_{01} - \omega_{12}| / \omega_{01}$ where $\mathcal{Q}_{01}$ is the quality factor of the $0 \to 1$ transition. Josephson tunnel junctions are crucial for quantum circuits since they bring a strongly non-parabolic inductive potential energy.

4 The Josephson non-linear inductance

At low temperatures, and at the low voltages and low frequencies corresponding to quantum information manipulation, the Josephson tunnel junction behaves as a pure non-linear inductance (Josephson element) in parallel with the capacitance corresponding to the parallel plate capacitor formed by the two overlapping films of the junction (Fig. 1b). This minimal, yet precise model, allows arbitrary complex quantum circuits to be analysed by a quantum version of conventional circuit theory. Even though the tunnel barrier is a layer of order ten atoms thick, the value of the Josephson non-linear inductance is very robust against static disorder, just like an ordinary inductance – such as the one considered in section 3 – is very insensitive to the position of each atom in the wire. We refer to [14] for a detailed discussion of this point.

4.1 Constitutive equation

Let us recall that a linear inductor, like any electrical element, can be fully characterized by its constitutive equation. Introducing a generalization of the ordinary magnetic flux, which is only defined for a loop, we define the **branch flux of an electric element** by $\Phi(t) = \int_{-\infty}^{t} V(t_1)dt_1$, where $V(t)$ is the space integral of the electric field along a current line inside the element. In this language, the current $I(t)$ flowing through the inductor is proportional to its branch flux $\Phi(t)$:

$$I(t) = \frac{1}{L}\Phi(t) \qquad (2)$$

Note that the generalized flux $\Phi(t)$ can be defined for any electric element with two leads (dipole element), and in particular for the Josephson junction, even though it does not resemble a coil. The Josephson element behaves inductively, as its branch flux-current relationship [5] is:

$$I(t) = I_0 \sin\left[2\pi\Phi(t)/\Phi_0\right] \qquad (3)$$

This inductive behavior is the manifestation, at the level of collective electrical variables, of the inertia of Cooper pairs tunneling across the insulator
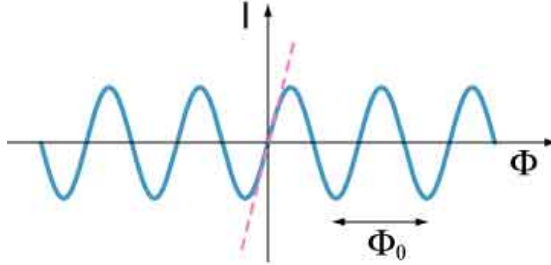
10

Figure 3: Sinusoidal current-flux relationship of a Josephson tunnel junction, the simplest non-linear, non-dissipative electrical element (solid line). Dashed line represents current-flux relationship for a linear inductance equal to the junction effective inductance.

(kinetic inductance). The discreteness of Cooper pair tunneling causes the periodic flux dependence of the current, with a period given by a universal quantum constant Φ_0, the superconducting flux quantum $h/2e$. The junction parameter I_0 is called the critical current of the tunnel element. It scales proportionally to the area of the tunnel layer and diminishes exponentially with the tunnel layer thickness. Note that the constitutive relation Eq. (3) expresses in only one equation the two Josephson relations [5]. This compact formulation is made possible by the introduction of the branch flux (see Fig. 3).

The purely sinusoidal form of the constitutive relation Eq. (3) can be traced to the perturbative nature of Cooper pair tunneling in a tunnel junction. Higher harmonics can appear if the tunnel layer becomes very thin, though their presence would not fundamentally change the discussion presented in this review. The quantity $2\pi\Phi(t)/\Phi_0 = \delta$ is called the gauge-invariant phase difference across the junction (often abridged into "phase"). It is important to realize that at the level of the constitutive relation of the Josephson element, this variable is nothing else than an electromagnetic flux in dimensionless units. In general, we have

$$\theta = \delta \bmod 2\pi$$

where θ is the phase difference between the two superconducting condensates on both sides of the junction. This last relation expresses how the superconducting ground state and electromagnetism are tied together.

4.2 Other forms of the parameter describing the Josephson non-linear inductance

The Josephson element is also often described by two other parameters, each of which carry exactly the same information as the critical current. The first one is the Josephson effective inductance $L_{J0} = \varphi_0/I_0$, where $\varphi_0 = \Phi_0/2\pi$ is

the reduced flux quantum. The name of this other form becomes obvious if we expand the sine function in Eq. (3) in powers of Φ around $\Phi = 0$. Keeping the leading term, we have $I = \Phi/L_{J0}$. Note that the junction behaves for small signals almost as a point-like kinetic inductance: a 100nm×100nm area junction will have a typical inductance of 100nH, whereas the same inductance is only obtained magnetically with a loop of about 1cm in diameter. More generally, it is convenient to define the phase-dependent Josephson inductance

$$L_J(\delta) = \left(\frac{\partial I}{\partial \Phi} \right)^{-1} = \frac{L_{J0}}{\cos \delta}$$

Note that the Josephson inductance not only depends on δ, it can actually become infinite or negative! Thus, under the proper conditions, the Josephson element can become a switch and even an active circuit element, as we will see below.

The other useful parameter is the Josephson energy $E_J = \varphi_0 I_0$. If we compute the energy stored in the junction $E(t) = \int_{-\infty}^{t} I(t_1) V(t_1) dt_1$, we find $E(t) = -E_J \cos[2\pi\Phi(t)/\Phi_0]$. In contrast with the parabolic dependence on flux of the energy of an inductance, the potential associated with a Josephson element has the shape of a cosine washboard. The total height of the corrugation of the washboard is $2E_J$.

4.3 Tuning the Josephson element

A direct application of the non-linear inductance of the Josephson element is obtained by splitting a junction and its leads into 2 equal junctions, such that the resulting loop has an inductance much smaller the Josephson inductance. The two smaller junctions in parallel then behave as an effective junction [15] whose Josephson energy varies with Φ_{ext}, the magnetic flux externally imposed through the loop:

$$E_J(\Phi_{\text{ext}}) = E_J \cos(\pi\Phi_{\text{ext}}/\Phi_0) \tag{4}$$

Here, E_J the total Josephson energy of the two junctions. The Josephson energy can also be modulated by applying a magnetic field in the plane parallel to the tunnel layer.

5 The quantum isolated Josephson junction

5.1 Form of the hamiltonian

If we leave the leads of a Josephson junction unconnected, we obtain the simplest example of a non-linear electrical resonator. In order to analyze its quantum dynamics, we apply the prescriptions of quantum circuit theory briefly summarized in Appendix A. Choosing a representation privileging the branch variables of the Josephson element, the momentum corresponds to the charge $Q = 2eN$

having tunneled through the element and the canonically conjugate position is the flux $\Phi = \varphi_0 \theta$ associated with the superconducting phase difference across the tunnel layer. Here, N and θ are treated as operators that obey $[\theta, N] = i$. It is important to note that the operator N has integer eigenvalues whereas the phase θ is an operator corresponding to the position of a point on the unit circle (an angle modulo 2π).

By eliminating the branch charge of the capacitor, the hamiltonian reduces to

$$H = E_{CJ} \left(N - Q_r/2e\right)^2 - E_J \cos \theta \tag{5}$$

where $E_{CJ} = \frac{(2e)^2}{2C_J}$ is the Coulomb charging energy corresponding to one Cooper pair on the junction capacitance C_J and where Q_r is the residual offset charge on the capacitor.

One may wonder how the constant Q_r got into the hamiltonian, since no such term appeared in the corresponding LC circuit in section 3. The continuous charge Q_r is equal to the charge that pre-existed on the capacitor when it was wired with the inductor. Such offset charge is not some nit-picking theoretical construct. Its physical origin is a slight difference in work function between the two electrodes of the capacitor and/or an excess of charged impurities in the vicinity of one of the capacitor plates relative to the other. The value of Q_r is in practice very large compared to the Cooper pair charge $2e$, and since the hamiltonian (5) is invariant under the transformation $N \rightarrow N \pm 1$, its value can be considered completely random.

Such residual offset charge also exists in the LC circuit. However, we did not include it in our description of section 3 since a time-independent Q_r does not appear in the dynamical behavior of the circuit: it can be removed from the hamiltonian by performing a trivial canonical transformation leaving the form of the hamiltonian unchanged.

It is not possible, however, to iron this constant out of the junction hamiltonian (5) because the potential is not quadratic in θ. The parameter Q_r plays a role here similar to the vector potential appearing in the hamiltonian of an electron in a magnetic field.

5.2 Fluctuations of the parameters of the hamiltonian

The hamiltonian (5) thus depends thus on three parameters which, following our discussion of the LC oscillator, we write as

$$
\begin{aligned}
Q_r &= Q_r^{\text{stat}} + \Delta Q_r(t) \\
E_C &= E_C^{\text{stat}} + \Delta E_C(t) \\
E_J &= E_J^{\text{stat}} + \Delta E_J(t)
\end{aligned}
\tag{6}
$$

in order to distinguish the static variation resulting from fabrication of the circuit from the time-dependent fluctuations. While Q_r^{stat} can be considered fully

random (see above discussion), E_C^{stat} and E_J^{stat} can generally be adjusted by construction to a precision better than 20%. The relative fluctuations $\Delta Q_r(t)/2e$ and $\Delta E_J(t)/E_J$ are found to have a $1/f$ power spectral density with a typical standard deviations at 1 Hz roughly of order 10^{-3} Hz$^{-1/2}$ and 10^{-5} Hz$^{-1/2}$, respectively, for a junction with a typical area of 0.01 μm^2 [16]. The noise appears to be produced by independent two-level fluctuators [17]. The relative fluctuations $\Delta E_C(t)/E_C$ are much less known, but the behavior of some glassy insulators at low temperatures might lead us to expect also a $1/f$ power spectral density, but probably with a weaker intensity than those of $\Delta E_J(t)/E_J$. We refer to the 3 noise terms in Eq. (6) as offset charge, dielectric and critical current noises, respectively.

6 Why three basic types of Josephson qubits?

The first-order problem in realizing a Josephson qubit is to suppress as much as possible the detrimental effect of the fluctuations of Q_r, while retaining the non-linearity of the circuit. There are three main stategies for solving this problem and they lead to three fundamental basic type of qubits involving only one Josephson element.

6.1 The Cooper pair box

The simplest circuit is called the "Cooper pair box" and was first described theoretically, albeit in a slightly different version than presented here, by M. Büttiker [18]. It was first realized experimentally by the Saclay group in 1997 [19]. Quantum dynamics in the time domain were first seen by the NEC group in 1999 [20].

In the Cooper pair box, the deviations of the residual offset charge Q_r are compensated by biasing the Josephson tunnel junction with a voltage source U in series with a "gate" capacitor C_g (see Fig. 4a). One can easily show that the hamiltonian of the Cooper pair box is

$$H = E_C\left(N - N_g\right)^2 - E_J\cos\theta \qquad (7)$$

Here $E_C = (2e)^2/\left(2\left(C_J + C_g\right)\right)$ is the charging energy of the island of the box and $N_g = Q_r + C_g U/2e$. Note that this hamiltonian has the same form as hamiltonian (5). Often N_g is simply written as $C_g U/2e$ since U at the chip level will anyway deviate substantially from the generator value at high-temperature due to stray emf's in the low-temperature cryogenic wiring.

In Fig. 5 we show the potential in the θ representation as well as the first few energy levels for $E_J/E_C = 1$ and $N_g = 0$. As shown in Appendix B, the Cooper pair box eigenenergies and eigenfunctions can be calculated with special functions known with arbitrary precision, and in Fig. 6 we plot the first few eigenenergies as a function of N_g for $E_J/E_C = 0.1$ and $E_J/E_C = 1$. Thus, the Cooper box is to quantum circuit physics what the hydrogen atom is to atomic physics. We can modify the spectrum with the action of two externally
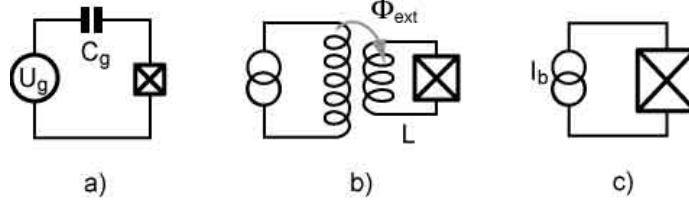
Figure 4: The three basic superconducting qubits. a) Cooper pair box (prototypal charge qubit), b) RF-SQUID (prototypal flux qubit) and c) current-biased junction (prototypal phase qubit). The charge qubit and the flux qubit requires small junctions fabricated with e-beam lithography while the phase qubit can be fabricated with conventional optical lithography.

controllable electrodynamic parameters: N_g, which is directly proportional to U, and E_J, which can be varied by applying a field through the junction or by using a split junction and applying a flux through the loop, as discussed in section 3. These parameters bear some resemblance to the Stark and Zeeman fields in atomic physics. For the box, however much smaller values of the fields are required to change the spectrum entirely.

We now limit ourselves to the two lowest levels of the box. Near the degeneracy point $N_g = 1/2$ where the electrostatic energy of the of the two charge states $|N = 0\rangle$ and $|N = 1\rangle$ are equal, we get the reduced hamiltonian [19, 21]

$$H_{\text{qubit}} = -E_z \left(\sigma_Z + X_{\text{control}} \sigma_X \right) \tag{8}$$

where, in the limit $E_J/E_C \ll 1$, $E_z = E_J/2$ and $X_{\text{control}} = 2E_C/E_J \left(1/2 - N_g \right)$. In Eq. (8), σ_Z and σ_X refer to the Pauli spin operators. Note that the X
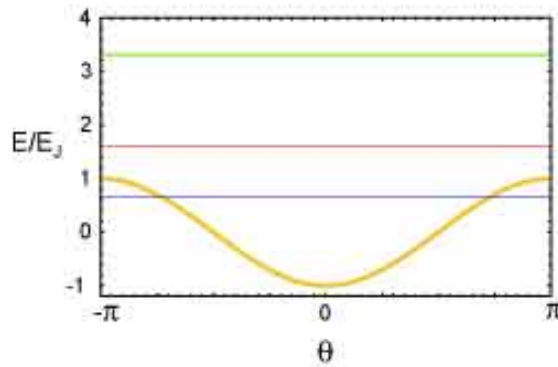
Figure 5: Potential landscape for the phase in a Cooper pair box (thick solid line). The first few levels for $E_J/E_C = 1$ and $N_g = 1/2$ are indicated by thin horizontal solid lines.

15
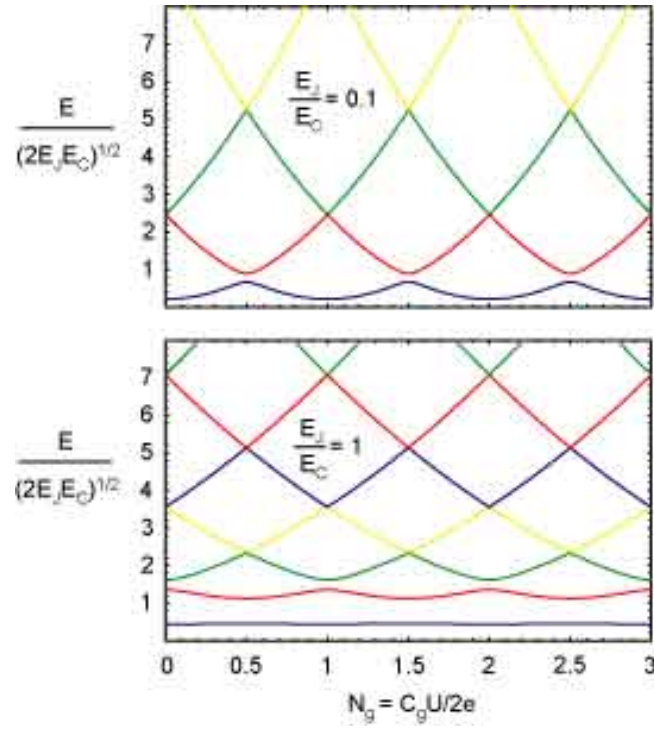
Figure 6: Energy levels of the Cooper pair box as a function of N_g, for two values of E_J/E_C. As E_J/E_C increases, the sensitivity of the box to variations of offset charge diminishes, but so does the non-linearity. However, the non-linearity is the slowest function of E_J/E_C and a compromise advantageous for coherence can be found.
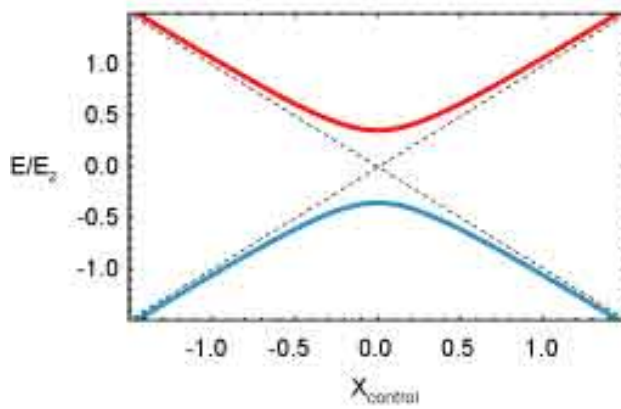
Figure 7: Universal level anticrossing found both for the Cooper pair box and the RF-SQUID at their "sweet spot".

direction is chosen along the charge operator, the variable of the box we can naturally couple to.

If we plot the energy of the eigenstates of (8) as a function of the control parameter X_{control}, we obtain the universal level repulsion diagram shown in Fig. 7. Note that the minimum energy splitting is given by E_J. Comparing Eq. (8) with the spin hamiltonian in NMR, we see that E_J plays the role of the Zeeman field while the electrostatic energy plays the role of the transverse field. Indeed we can send on the control port corresponding to U time-varying voltage signals in the form of NMR-type pulses and prepare arbitrary superpositions of states [22].

The expression (8) shows that at the "sweet spot" $X_{\text{control}} = 0$, i.e. the degeneracy point $N_g = 1/2$, the qubit transition frequency is to first order insentive to the offset charge noise ΔQ_r. We will discuss in the next section how an extension of the Cooper pair box circuit can display quantum coherence properties on long time scales by using this property.

In general, circuits derived from the Cooper pair box have been nicknamed "charge qubits". One should not think, however, that in charge qubits, quantum information is *encoded* with charge. Both the charge N and phase θ are quantum variables and they are both uncertain for a generic quantum state. Charge in "charge qubits" should be understood as refering to the "controlled variable", i.e. the qubit variable that couples to the control line we use to write or manipulate quantum information. In the following, for better comparison between the three qubits, we will be faithful to the convention used in Eq. (8), namely that σ_X represents the *controlled variable*.
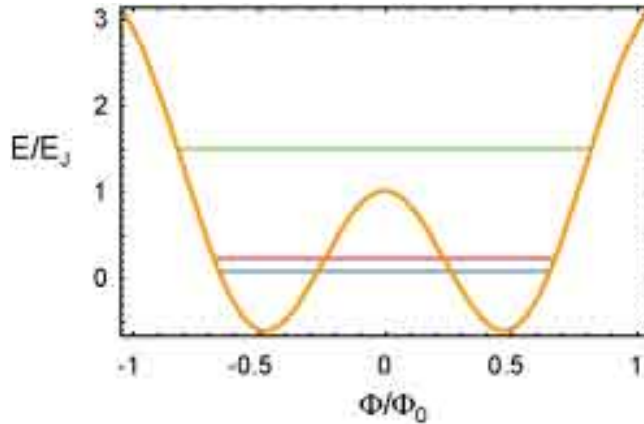
17

Figure 8: Schematic potential energy landcape for the RF-SQUID.

6.2 The RF-SQUID

The second circuit – the so-called RF-SQUID [23] – can be considered in several ways the dual of the Cooper pair box (see Fig. 4b). It employs a superconducting transformer rather than a gate capacitor to adjust the hamiltonian. The two sides of the junction with capacitance C_J are connected by a superconducting loop with inductance L. An external flux Φ_{ext} is imposed through the loop by an auxiliary coil. Using the methods of Appendix A, we obtain the hamiltonian [8]

$$H = \frac{q^2}{2C_J} + \frac{\phi^2}{2L} - E_J \cos\left[\frac{2e}{\hbar}\left(\phi - \Phi_{\text{ext}}\right)\right] \tag{9}$$

We are taking here as degrees of freedom the integral ϕ of the voltage across the inductance L, i.e. the flux through the superconducting loop, and its conjugate variable, the charge q on the capacitance C_J; they obey $[\phi, q] = i\hbar$. Note that in this representation, the phase θ, corresponding to the branch flux across the Josephson element, has been eliminated. Note also that the flux ϕ, in contrast to the phase θ, takes its values on a line and not on a circle. Likewise, its conjugate variable q, the charge on the capacitance, has continuous eigenvalues and not integer ones like N. Note that we now have three adjustable energy scales: E_J, $E_{CJ} = (2e)^2/2C_J$ and $E_L = \Phi_0^2/2L$.

The potential in the flux representation is schematically shown in Fig. 8 together with the first few levels, which have been seen experimentally for the first time by the SUNY group [24]. Here, no analytical expressions exist for the eigenvalues and the eigenfunctions of the problem, which has two aspect ratios: E_J/E_{CJ} and $\lambda = L_J/L - 1$.

Whereas in the Cooper box the potential is cosine-shaped and has only one well since the variable θ is 2π-periodic, we have now in general a parabolic

18

potential with a cosine corrugation. The idea here for curing the detrimental effect of the offset charge fluctuations is very different than in the box. First of all Q_r^{stat} has been neutralized by shunting the 2 metallic electrodes of the junction by the superconducting wire of the loop. Then, the ratio E_J/E_{CJ} is chosen to be much larger than unity. This tends to increase the relative strength of quantum fluctuations of q, making offset charge fluctuations ΔQ_r small in comparison. The resulting loss in the non-linearity of the first levels is compensated by taking λ close to zero and by flux-biasing the device at the half-flux quantum value $\Phi_{\text{ext}} = \Phi_0/2$. Under these conditions, the potential has two degenerate wells separated by a shallow barrier with height $E_B = E_J 3\lambda^2/2$. This corresponds to the degeneracy value $N_g = 1/2$ in the Cooper box, with the inductance energy in place of the capacitance energy. At $\Phi_{\text{ext}} = \Phi_0/2$, the two lowest energy levels are then the symmetric and antisymmetric combinations of the two wavefunctions localized in each well, and the energy splitting between the two states can be seen as the tunnel splitting associated with the quantum motion through the potential barrier between the two wells, bearing close resemblance to the dynamics of the ammonia molecule. This splitting E_S depends exponentially on the barrier height, which itself depends strongly on E_J. We have $E_S = \eta\sqrt{E_B E_{CJ}}\exp\left(-\xi\sqrt{E_B/E_{CJ}}\right)$ where the numbers η and ξ have to be determined numerically in most practical cases. The non-linearity of the first levels results thus from a subtle cancellation between two inductances: the superconducting loop inductance L and the junction effective inductance $-L_{J0}$ which is opposed to L near $\Phi_{\text{ext}} = \Phi_0/2$. However, as we move away from the degeneracy point $\Phi_{\text{ext}} = \Phi_0/2$, the splitting $2E_\Phi$ between the first two energy levels varies linearly with the applied flux $E_\Phi = \zeta E_L (N_\Phi - 1/2)$. Here the parameter $N_\Phi = \Phi_{\text{ext}}/\Phi_0$, also called the flux frustration, plays the role of the reduced gate charge N_g. The coefficient ζ has also to be determined numerically. We are therefore again, in the vicinity of the flux degeneracy point $\Phi_{\text{ext}} = \Phi_0/2$ and for $E_J/E_{CJ} \gg 1$, in presence of the universal level repulsion behavior (see Fig. 7) and the qubit hamiltonian is again given by

$$H_{qubit} = -E_z \left(\sigma_Z + X_{\text{control}}\sigma_X \right) \tag{10}$$

where now $E_z = E_S/2$ and $X_{\text{control}} = 2\zeta E_L/E_S (1/2 - N_\Phi)$. The qubits derived from this basic circuit [25, 33] have been nicknamed "flux qubits". Again, quantum information is not directly represented here by the flux ϕ, which is as uncertain for a general qubit state as the charge q on the capacitor plates of the junction. The flux ϕ is the system variable to which we couple when we write or control information in the qubit, which is done by sending current pulses on the primary of the RF-SQUID transformer, thereby modulating N_Φ, which itself determines the strength of the pseudo-field in the X direction in the hamiltonian (10). Note that the parameters E_S, E_Φ, and N_Φ are all influenced to some degree by the critical current noise, the dielectric noise and the charge noise. Another independent noise can also be present, the noise of the flux in the loop, which is not found in the box and which will affect only N_Φ. Experiments

19

on DC-SQUIDS [15] have shown that this noise, in adequate conditions, can be as low as $10^{-8}(h/2e)\mathrm{Hz}^{-1/2}$ at a few kHz. However, experimental results on flux qubits (see below) seem to indicate that larger apparent flux fluctuations are present, either as a result of flux trapping or critical current fluctuations in junctions implementing inductances.

6.3 Current-biased junction

The third basic quantum circuit biases the junction with a fixed DC-current source (Fig. 7c). Like the flux qubit, this circuit is also insensitive to the effect of offset charge and reduces the effect of charge fluctuations by using large ratios of E_J/E_{CJ}. A large non-linearity in the Josephson inductance is obtained by biasing the junction at a current I very close to the critical current. A current bias source can be understood as arising from a loop inductance with $L \to \infty$ biased by a flux $\Phi \to \infty$ such that $I = \Phi/L$. The Hamiltonian is given by

$$H = E_{CJ}p^2 - I\varphi_0\delta - I_0\varphi_0\cos\delta \ , \tag{11}$$

where the gauge invariant phase difference operator δ is, apart from the scale factor φ_0, precisely the branch flux across C_J. Its conjugate variable is the charge $2ep$ on that capacitance, a continuous operator. We have thus $[\delta, p] = i$. The variable δ, like the variable ϕ of the RF-SQUID, takes its value on the whole real axis and its relation with the phase θ is $\delta \bmod 2\pi = \theta$ as in our classical analysis of section 4.

The potential in the δ representation is shown in Fig. 9. It has the shape of a tilted washboard, with the tilt given by the ratio I/I_0. When I approaches I_0, the phase is $\delta \approx \pi/2$, and in its vicinity, the potential is very well approximated by the cubic form

$$U\left(\delta\right) = \varphi_0\left(I_0 - I\right)\left(\delta - \pi/2\right) - \frac{I_0\varphi_0}{6}\left(\delta - \pi/2\right)^3 \tag{12}$$

Note that its shape depends critically on the difference $I_0 - I$. For $I \lesssim I_0$, there is a well with a barrier height $\Delta U = (2\sqrt{2}/3)I_0\varphi_0\left(1 - I/I_0\right)^{3/2}$ and the classical oscillation frequency at the bottom of the well (so-called plasma oscillation) is given by

$$
\begin{aligned}
\omega_p &= \frac{1}{\sqrt{L_J(I)C_J}} \\
&= \frac{1}{\sqrt{L_{J0}C_J}}\left[1 - (I/I_0)^2\right]^{1/4}
\end{aligned}
$$

Quantum-mechanically, energy levels are found in the well (see Fig. 11) [3] with non-degenerate spacings. The first two levels can be used for qubit states [26], and have a transition frequency $\omega_{01} \simeq 0.95\,\omega_p$.

A feature of this qubit circuit is built-in readout, a property missing from the two previous cases. It is based on the possibility that states in the cubic potential
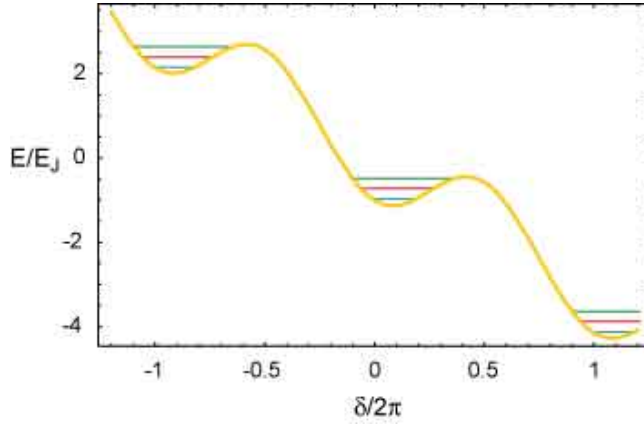
Figure 9: Tilted washboard potential of the current-biased Josephson junction.

can tunnel through the cubic potential barrier into the continuum outside the barrier. Because the tunneling rate increases by a factor of approximately 500 each time we go from one energy level to the next, the population of the $|1\rangle$ qubit state can be reliably measured by sending a probe signal inducing a transition from the 1 state to a higher energy state with large tunneling probability. After tunneling, the particle representing the phase accelerates down the washboard, a convenient self-amplification process leading to a voltage $2\Delta/e$ across the junction. Therefore, a finite voltage $V \neq 0$ suddenly appearing across the junction just after the probe signal implies that the qubit was in state $|1\rangle$, whereas $V = 0$ implies that the qubit was in state $|0\rangle$.

In practice, like in the two previous cases, the transition frequency $\omega_{01}/2\pi$ falls in the 5-20 GHz range. This frequency is only determined by material properties of the barrier, since the product $C_J L_J$ does not depend on junction area. The number of levels in the well is typically $\Delta U/\hbar\omega_p \approx 4$.

Setting the bias current at a value I and calling ΔI the variations of the difference $I - I_0$ (originating either in variations of I or I_0), the qubit Hamiltonian is given by

$$H_{\text{qubit}} = \frac{\hbar\omega_{01}}{2}\sigma_Z + \sqrt{\frac{\hbar}{2\omega_{01}C_J}}\Delta I(\sigma_X + \chi\sigma_Z), \tag{13}$$

where $\chi = \sqrt{\hbar\omega_{01}/3\Delta U} \simeq 1/4$ for typical operating parameters. In contrast with the flux and phase qubit circuits, the current-biased Josephson junction does not have a bias point where the $0\rightarrow1$ transition frequency has a local minimum. The hamiltonian cannot be cast into the NMR-type form of Eq. (8). However, a sinusoidal current signal $\Delta I(t) \sim \sin\omega_{01}t$ can still produce σ_X rotations, whereas a low-frequency signal produces σ_Z operations [27].

In analogy with the preceding circuits, qubits derived from this circuit and/or having the same phase potential shape and qubit properties have been

nicknamed "phase qubits" since the controlled variable is the phase (the X pseudo-spin direction in hamiltonian (13)).

6.4   Tunability versus sensitivity to noise in control parameters

The reduced two-level hamiltonians Eqs. (8,10) and (13) have been tested thoroughly and are now well-established. They contain the very important parametric dependence of the coefficient of σ_X, which can be viewed on one hand as how much the qubit can be tuned by an external control parameter, and on the other hand as how much it can be dephased by uncontrolled variations in that parameter. It is often important to realize that even if the control parameter has a very stable value at the level of room-temperature electronics, the noise in the electrical components relaying its value at the qubit level might be inducing detrimental fluctuations. An example is the flux through a superconducting loop, which in principle could be set very precisely by a stable current in a coil, and which in practice often fluctuates because of trapped flux motion in the wire of the loop or in nearby superconducting films. Note that, on the other hand, the two-level hamiltonian does not contain all the non-linear properties of the qubit, and how they conflict with its intrinsic noise, a problem which we discuss in the next subsection.

6.5   Non-linearity versus sensitivity to intrinsic noise

The three basic quantum circuit types discussed above illustrate a general tendency of Josephson qubits. If we try to make the level structure very non-linear, i.e. $|\omega_{01} - \omega_{12}| \gg \omega_{01}$, we necessarily expose the system sensitively to at least one type of intrinsic noise. The flux qubit is contructed to reach a very large non-linearity, but is also maximally exposed, relatively speaking, to critical current noise and flux noise. On the other hand, the phase qubit starts with a relatively small non-linearity and acquires it at the expense of a precise tuning of the difference between the bias current and the critical current, and therefore exposes itself also to the noise in the latter. The Cooper pair box, finally, acquires non-linearity at the expense of its sensitivity to offset charge noise. The search for the optimal qubit circuit involves therefore a detailed knowledge of the relative intensities of the various sources of noise, and their variations with all the construction parameters of the qubit, and in particular – this point is crucial – the properties of the materials involved in the tunnel junction fabrication. Such in-depth knowledge does not yet exist at the time of this writing and one can only make educated guesses.

The qubit optimization problem is also further complicated by the necessity to readout quantum information, which we address just after reviewing the relationships between the intensity of noise and the decay rates of quantum information.

7 Qubit relaxation and decoherence

A generic quantum state of a qubit can be represented as a unit vector $\overrightarrow{S}$ pointing on a sphere – the so-called Bloch sphere. One distinguishes two broad classes of errors. The first one corresponds to the tip of the Bloch vector diffusing in the latitude direction, i.e. along the arc joining the two poles of the sphere to or away from the North pole. This process is called energy relaxation or state-mixing. The second class corresponds to the tip of the Bloch vector diffusing in the longitude direction, i.e. perpendicularly to the line joining the two poles. This process is called dephasing or decoherence.

In Appendix C we define precisely the relaxation and decoherence rates and show that they are directly proportional to the power spectral densities of the noises entering in the parameters of the hamiltonian of the qubit. More precisely, we find that the decoherence rate is proportional to the total spectral density of the quasi-zero-frequency noise in the qubit Larmor frequency. The relaxation rate, on the other hand, is proportional to the total spectral density, at the qubit Larmor frequency, of the noise in the field perpendicular to the eigenaxis of the qubit.

In principle, the expressions for the relaxation and decoherence rate could lead to a ranking of the various qubit circuits: from their reduced spin hamiltonian, one can find with what coefficient each basic noise source contributes to the various spectral densities entering in the rates. In the same manner, one could optimize the various qubit parameters to make them insensitive to noise, as much as possible. However, before discussing this question further, we must realize that the readout itself can provide substantial additional noise sources for the qubit. Therefore, the design of a qubit circuit that maximizes the number of coherent gate operations is a subtle optimization problem which must treat in parallel both the intrinsic noises of the qubit and the back-action noise of the readout.

8 Readout of superconducting qubits

8.1 Formulation of the readout problem

We have examined so far the various basic circuits for qubit implementation and their associated methods to write and manipulate quantum information. Another important task quantum circuits must perform is the readout of that information. As we mentioned earlier, the difficulty of the readout problem is to open a coupling channel to the qubit for extracting information without at the same time submitting it to noise.

Ideally, the readout part of the circuit – referred to in the following simply as "readout" – should include both a switch, which defines an "OFF" and an "ON" phase, and a state measurement device. During the OFF phase, where reset and gate operations take place, the measurement device should be completely decoupled from the qubit degrees of freedom. During the ON phase,

the measurement device should be maximally coupled to a qubit variable that distinguishes the 0 and the 1 state. However, this condition is not sufficient. The back-action of the measurement device during the ON phase should be weak enough not to relax the qubit [28].

The readout can be characterized by 4 parameters. The first one describes the sensitivity of the measuring device while the next two describe its back-action, factoring in the quality of the switch:

i) the measurement time τ_m defined as the time taken by the measuring device to reach a signal-to-noise ratio of 1 in the determination of the state.

ii) the energy relaxation rate Γ_1^{ON} of the qubit in the ON state.

iii) the coherence decay rate Γ_2^{OFF} of the qubit information in the OFF state.

iv) the dead time t_d needed to reset both the measuring device and qubit after a measurement. They are usually perturbed by the energy expenditure associated with producing a signal strong enough for external detection.

Simultaneously minimizing these parameters to improve readout performance cannot be done without running into conflicts. An important quantity to optimize is the readout fidelity. By construction, at the end of the ON phase, the readout should have reached one of two classical states: 0_c and 1_c, the outcomes of the measurement process. The latter can be described by 2 probabilities: the probability $p_{00_c}(p_{11_c})$ that starting from the qubit state $|0\rangle$ $(|1\rangle)$ the measurement yields $0_c(1_c)$. The readout fidelity (or discriminating power) is defined as $F = p_{00c} + p_{11_c} - 1$. For a measuring device with a signal-to-noise ratio increasing like the measurement duration τ, we would have, if back-action could be neglected, $F = \mathrm{erf}\left(2^{-1/2}\sqrt{\tau/\tau_{\mathrm{m}}}\right)$.

8.2 Requirements and general strategies

The fidelity and speed of the readout, usually not discussed in the context of quantum algorithms because they enter marginally in the evaluation of their complexity, are actually key to experiments studying the coherence properties of qubits and gates. A very fast and sensitive readout will gather at a rapid pace information on the imperfections and drifts of qubit parameters, thereby allowing the experimenter to design fabrication strategies to fight them during the construction or even correct them in real time.

We are thus mostly interested in "single-shot" readouts [28], for which F is of order unity, as opposed to schemes in which a weak measurement is performed continuously [29]. If $F \ll 1$, of order F^{-2} identical preparation and readout cycles need to be performed to access the state of the qubit. The condition for "single-shot" operation is

$$\Gamma_1^{\mathrm{ON}}\tau_m < 1$$

The speed of the readout, determined both by τ_m and t_d, should be sufficiently fast to allow a complete characterization of all the properties of the qubit before any drift in parameters occurs. With sufficient speed, the automatic correction of these drits in real time using feedback will be possible.

Rapidly pulsing the readout on and off with a large decoupling amplitude such that

$$\Gamma_2^{\mathrm{OFF}} T_2 \ll 1$$

requires a fast, strongly non-linear element, which is provided by one or more auxiliary Josephson junctions. Decoupling the qubit from the readout in the OFF phase requires balancing the circuit in the manner of a Wheatstone bridge, with the readout input variable and the qubit variable corresponding to 2 orthogonal electrical degrees of freedom. Finally, to be as complete as possible even in presence of small asymmetries, the decoupling also requires an impedance mismatch between the qubit and the dissipative degrees of freedom of the readout. In the next subsection, we discuss how these general ideas have been implemented in 2nd generation quantum circuits. The first three examples we have chosen involve a readout circuit which is built-in the qubit itself to provide maximal coupling during the ON phase, as well as a decoupling scheme which has proven effective for obtaining long decoherence times. The last example incorporates a novel dispersive readout.

8.3 Phase qubit: tunneling readout with a DC-SQUID on-chip amplifier.

The simplest example of a readout is provided by a system derived from the phase qubit (See Fig. 10). In the phase qubit, the levels in the cubic potential are metastable and decay in the continuum, with level $n+1$ having roughly a decay rate Γ_{n+1} 500 times faster than the decay Γ_n of level n. This strong level number dependence of the decay rate leads naturally to the following readout scheme: when readout needs to be performed, a microwave pulse at the transition frequency ω_{12} (or better at ω_{13}) transfers the eventual population of level 1 into level 2, the latter decaying rapidly into the continuum, where it subsequently loses energy by friction and falls into the bottom state of the next corrugation of the potential (because the qubit junction is actually in a superconducting loop of large but finite inductance, the bottom of this next corrugation is in fact the absolute minimum of the potential and the particle representing the system can stay an infinitely long time there). Thus, at the end of the readout pulse, the sytem has either decayed out of the cubic well (readout state 1_c) if the qubit was in the $|1\rangle$ state or remained in the cubic well (readout state 0_c) if the qubit was in the $|0\rangle$ state. The DC-SQUID amplifier is sensitive enough to detect the change in flux accompanying the exit of the cubic well, but the problem is to avoid sending the back-action noise of its stabilizing resistor into the qubit circuit. The solution to this problem involves balancing
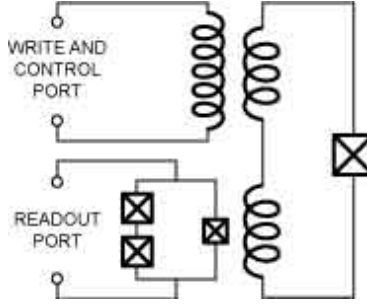
Figure 10: Phase qubit implemented with a Josephson junction in a high-inductance superconducting loop biased with a flux sufficiently large that the phase across the junction sees a potential analogous to that found for the current-biased junction. The readout part of the circuit is an asymmetric hysteretic SQUID which is completely decoupled from the qubit in the OFF phase. Isolation of the qubit both from the readout and control port is obtained through impedance mismatch of transformers.

the SQUID loop in such a way, that for readout state 0_c, the small signal gain of the SQUID is zero, whereas for readout state 1_c, the small signal gain is non-zero [17]. This signal dependent gain is obtained by having 2 junctions in one arm of the SQUID whose total Josephson inductance equals that of the unique junction in the other arm. Finally, a large impedance mismatch between the SQUID and the qubit is obtained by a transformer. The fidelity of such readout is remarkable: 95% has been demonstrated. In Fig. 11, we show the result of a measurement of Rabi oscillations with such qubit plus readout.

8.4 Cooper-pair box with non-linear inductive readout: the "Quantronium" circuit

The Cooper-pair box needs to be operated at its "sweet spot" (degeneracy point) where the transition frequency is to first order insensitive to offset charge fluctuations. The "Quantronium" circuit presented in Fig. 12 is a 3-junction bridge configuration with two small junctions defining a Cooper box island, and thus a charge-like qubit which is coupled capacitively to the write and control port (high-impedance port). There is also a large third junction, which provides a non-linear inductive coupling to the read port. When the read port current I is zero, and the flux through the qubit loop is zero, noise coming from the read port is decoupled from the qubit, provided that the two small junctions are identical both in critical current and capacitance. When I is non-zero, the junction bridge is out of balance and the state of the qubit influences the effective non-linear inductance seen from the read port. A further protection of the impedance mismatch type is obtained by a shunt capacitor across the large junction: at the resonance frequency of the non-linear resonator formed by the large junction and the external capacitance C, the differential mode of
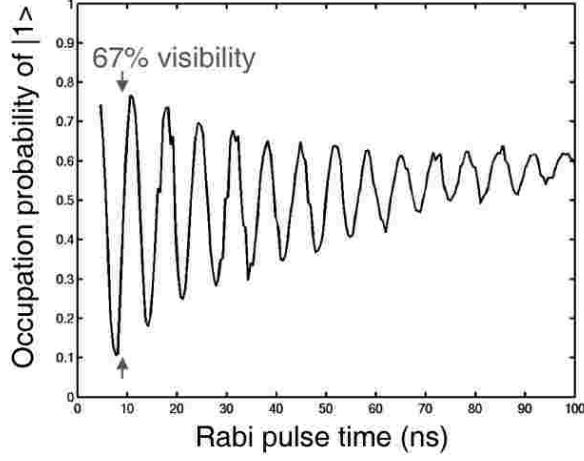
26

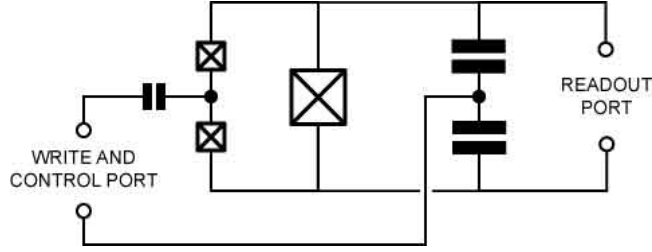Figure 11: Rabi oscillations observed for the qubit of Fig. 10.

Figure 12: "Quantronium" circuit consisting of a Cooper pair box with a non-linear inductive readout. A Wheatstone bridge configuration decouples qubit and readout variables when readout is OFF. Impedance mismatch isolation is also provided by additional capacitance in parallel with readout junction.

the circuit involved in the readout presents an impedance of the order of an ohm, a substantial decoupling from the 50 Ω transmission line carrying information to the amplifier stage. The readout protocol involves a DC pulse [30, 22] or an RF pulse [31] stimulation of the readout mode. The response is bimodal, each mode corresponding to a state of the qubit. Although the theoretical fidelity of the DC readout can attain 95%, only a maximum of 40% has been obtained so far. The cause of this discrepancy is still under investigation.

In Fig. 13 we show the result of a Ramsey fringe experiment demonstrating that the coherence quality factor of the quantronium can reach 25 000 at the sweet spot [22]. By studying the degradation of the qubit absorption line and of the Ramsey fringes as one moves away from the sweet spot, it has been possible to show that the residual decoherence is limited by offset charge noise and by flux noise [32]. In principle, the influence of these noises could be further reduced
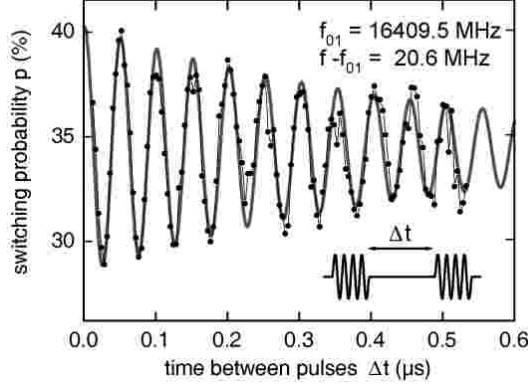
Figure 13: Measurement of Ramsey fringes for the Quantronium. Two $\pi/2$ pulses separated by a variable delay are applied to the qubit before measurement. The frequency of the pulse is slightly detuned from the transition frequency to provide a stroboscopic measurement of the Larmor precession of the qubit.

by a better optimization of the qubit design and parameters. In particular, the operation of the box can tolerate ratios of E_J/E_C around 4 where the sensitivity to offset charge is exponentially reduced and where the non-linearity is still of order 15%. The quantronium circuit has so far the best coherence quality factor. We believe this is due to the fact that critical current noise, one dominant intrinsic source of noise, affects this qubit far less than the others, relatively speaking, as can be deduced from the qubit hamiltonians of section 6.

8.5   3-junction flux qubit with built-in readout

Fig. 14 shows a third example of built-in readout, this time for a flux-like qubit. The qubit by itself involves 3 junctions in a loop, the larger two of the junctions playing the role of the loop inductance in the basic RF-SQUID [33]. The advantage of this configuration is to reduce the sensitivity of the qubit to external flux variations. The readout part of the circuit involves 2 other junctions forming a hysteretic DC-SQUID whose offset flux depends on the qubit flux state. The critical current of this DC-SQUID has been probed by a DC pulse, but an RF pulse could be applied as in another flux readout. Similarly to the two previous cases, the readout states 1_c and 0_c, which here correspond to the DC-SQUID having switched or not, map very well the qubit states $|1\rangle$ and $|0\rangle$, with a fidelity better than 60%. Here also, a bridge technique orthogonalizes the readout mode, which is the common mode of the DC-SQUID, and the qubit mode, which is coupled to the loop of the DC-SQUID. External capacitors provide additional protection through impedance mismatch. Fig. 15 shows Ramsey oscillations obtained with this system.
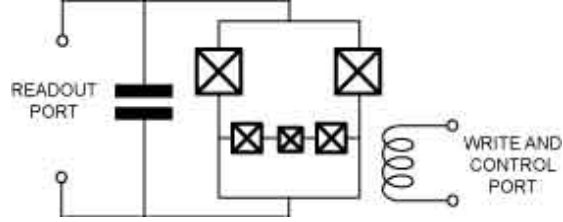
Figure 14: Three-junction flux qubit with a non-linear inductive readout. The medium-size junctions play the role of an inductor. Bridge configuration for nulling out back-action of readout is also employed here, as well as impedance mismatch provided by additional capacitance.
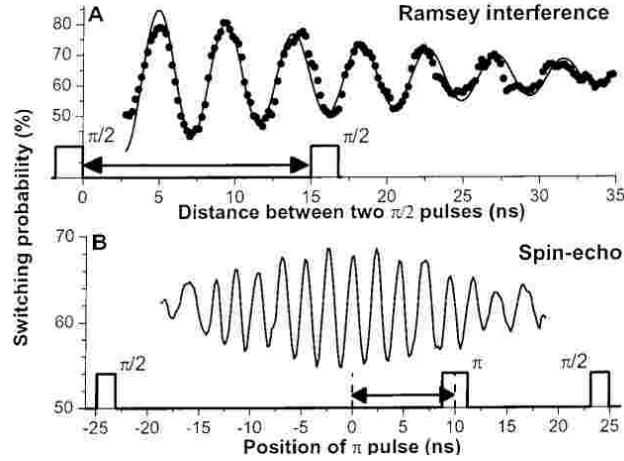

Figure 15: Ramsey fringes obtained for qubit of Fig. 14.

8.6 Avoiding on-chip dissipation with dispersive readout schemes

All the circuits above include an on-chip amplification scheme producing high-level signals which can be read directly by high-temperature low-noise electronics. In the second and third examples, these signals lead to non-equilibrium quasiparticle excitations being produced in the near vicinity of the qubit junctions. More generally, one can legitimately worry that large energy dissipation on the chip itself will lead to an increase of the noises discussed in section 5.2. A broad class of new readout schemes addresses this question [34, 31, 35]. They are based on a purely dispersive measurement of a qubit susceptibility (capacitive or inductive). A probe signal is sent to the qubit. The signal is coupled to a qubit variable whose average value is identical in the 2 qubit states (for instance, in the capacitive susceptibility, the variable is the island charge in the charge qubit at the degeneracy point). However, the susceptibility, which is the derivative of the qubit variable with respect to the probe, differs from one qubit state to the other. The resulting state-dependent phase shift of the reflected signal is thus amplified by a linear low-temperature amplifier and finally discriminated at high temperature against an adequately chosen threshold. In addition to being very thrifty in terms of energy being dissipated on chip, these new schemes also provide a further natural decoupling action: when the probe signal is off, the back-action of the amplifier is also completely shut off. Finally, the interrogation of the qubit in a frequency band excluding zero facilitates the design of very efficient filters.

8.7 Cooper-pair box with circuit quantum electrodynamics readout

As a representative example of the novel class of dispersive qubit readout schemes we discuss the circuit quantum electrodynamics architecture [34] applied to the readout of charge qubits in some more detail. In this approach a split Cooper pair box is capacitively coupled to a single mode of the electromagnetic field contained in a high quality on-chip transmission line resonator, see Fig. 16. Exciting the resonator at its full wave resonance frequency, the electric field has an antinode at the center of the resonator to which the qubit is strongly coupled by a large capacitance C_{g}. It has been demonstrated that the coupling can be made so large that a single photon in the transmission line can resonantly drive Rabi oscillations in the Cooper pair box at frequencies in excess of $10\,\mathrm{MHz}$ [36]. This rate of coherent exchange of a single excitation between the Cooper pair box and the resonator is much larger than the rates at which the Cooper pair box decoheres or the photon gets lost from the resonator. When the qubit transition frequency is detuned form the resonator, the mutual strong coupling gives rise to a qubit state-dependent frequency shift in the resonator transition frequency. This frequency shift can be used to perform a quantum non-demolition (QND) measurement of the qubit state by measuring the amplitude and phase of a probe microwave transmitted through the resonator at its bare resonance
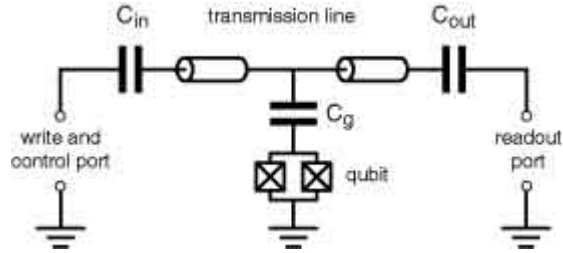
Figure 16: Circuit quantum electrodynamics architecture for readout of a Cooper pair box. The Cooper pair box is coupled capacitively (C_{g}) to a transmission line resonator with capacitively coupled input (C_{in}) and output (C_{out}) ports. The input port is used to control the qubit state using microwave pulses and to apply the readout microwave which, after transmission through the circuit, is detected at the readout port.

frequency [36, 37]. In this dispersive scheme, the susceptibility of the Cooper pair box which is maximal at charge degeneracy (the optimal bias point) is measured. The measurement is performed without dissipating any power in the circuit and thus minimizing the back-action. The only source of back-action in this QND measurement is the dephasing induced by the fluctuating ac-Stark shift in the qubit level separation due to the photon shot noise in the microwave readout beam [37]. In the detuned case, the resonator also enhances the qubit radiative lifetime by providing an impedance transformation which effectively filters out the noise of the electromagnetic environment at the qubit transition frequency. Using this architecture, it has been demonstrated that the quantum state of the Cooper pair box can be manipulated by applying microwave pulses at the qubit transition frequency to the write and control port of the circuit QED system. A measurement of Ramsey oscillations, showing a coherence time of $T_2 \sim 300$ ns at the optimal bias point, under a weak continuous probe beam is shown in Fig. 17.

9   Coupling superconducting qubits

A priori, 3 types of coupling schemes can be envisioned:

a) In the first type, the transition frequency of the qubits are all equal and the coupling between any pair is switched on using one or several junctions as non-linear elements [38, 39].

b) In the second type, the couplings are fixed, but the transition frequencies of a pair of qubits, originally detuned, are brought on resonance when the coupling between them needs to be turned on [40, 41, 42].

c) In the third type, which bears close resemblance to the methods used in NMR [1], the couplings and the resonance frequencies of the qubits
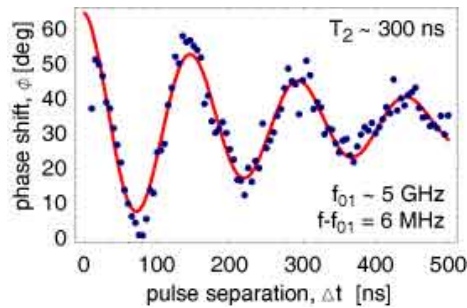
Figure 17: Ramsey oscillations observed in the phase of the transmitted probe beam in the circuit QED readout architecture. The drive frequency is detuned by 6 MHz from the qubit transition frequency. A dephasing time of $T_2 \sim 300$ ns is observed.

remain fixed, the qubits being always detuned. Being off-diagonal, the coupling elements have negligible action on the qubits. However, when a strong microwave field is applied to the target and control qubits at their resonant frequency and for an appropriate amplitude, they become in "speaking terms" for the exchange of energy quanta and gate action can take place [43].

So far only scheme b) has been tested experimentally.

The advantage of schemes b) and c) is that they work with purely passive reactive elements like capacitors and inductors which should remain very stable as a function of time and which also should present very little high-frequency noise. In a way, we must design quantum integrated circuits in the manner that vacuum tube radios were designed in the 50's: only 6 tubes were used for a complete heterodyne radio set, including the power supply. Nowadays several hundreds of transistors are used in a radio or any hi-fi system. In that ancient era of classical electronics, linear elements like capacitors, inductors or resistors were "free" because they were relatively reliable whereas tubes could break down easily. We have to follow a similar path in quantum integrated circuit, the reliability issues having become noise minimization issues.

10   Can coherence be improved with better materials?

Up to now, we have discussed how, given the power spectral densities of the noises ΔQ_r, ΔE_C and ΔE_J, we could design a qubit equipped with control, readout and coupling circuits. It is worthwhile to ask at this point if we could improve the material properties to improve the coherence of the qubit, assuming all other problems like noise in the control channels and the back-action of the readout have been solved. A model put forward by one of us (JMM)

and collaborators shed some light on the direction one would follow to answer this question. The $1/f$ spectrum of the materials noises suggests that they all originate from 2-level fluctuators in the amorphous alumina tunnel layer of the junction itself, or its close vicinity. The substrate or the surface of the superconducting films are also suspect in the case of ΔQ_r and ΔE_C but their influence would be relatively weaker and we ignore them for simplicity. These two-level systems are supposed to be randomly distributed positional degrees of freedom ξ_i with effective spin-1/2 properties, for instance an impurity atom tunneling between two adjacent potential wells. Each two-level system is in principle characterized by 3 parameters: the energy splitting $\hbar\omega_i$, and the two coefficients α_i and β_i of the Pauli matrix representation of $\xi_i = \alpha_i \sigma_{iz} + \beta_i \sigma_{ix}$ (z here is by definition the energy eigenbasis). The random nature of the problem leads us to suppose that α_i and β_i are both Gaussian random variables with the same standard deviation ρ_i. By carrying a charge, the thermal and quantum motion of ξ_i can contribute to $\Delta Q_r = \sum_i q_i \xi_i$ and $\Delta E_C = \sum_i c_i \beta_i^2 / \omega_i\, \sigma_{iz}$. Likewise, by modifying the transmission of a tunneling channel in its vicinity, the motion of ξ_i can contribute to $\Delta E_J = \sum_i g_i \xi_i$. We can further suppose that the quality of the material of the junction is simply characterized by a few numbers. The essential one is the density ν of the transition frequencies ω_i in frequency space and in real space, assuming a ω^{-1} distribution (this is necessary to explain the $1/f$ behavior) and a uniform spatial distribution on the surface of the junction. Recent experiments indicate that the parameter ν is of order $10^5\,\mu\mathrm{m}^{-2}(\mathrm{decade})^{-1}$. Then, assuming a universal value for $\rho = \langle \rho_i \rangle$ which is independent of frequency, only one coefficient is needed per noise, namely, the average modulation efficiency of each fluctuator. Such analysis provides a common language for describing various experiments probing the dependence of decoherence on the material of the junction. Once the influence of the junction fabrication parameters (oxidation pressure and temperature, impurity contents, and so on) on these noise intensities will be known, it will be possible to devise optimized fabrication procedures, in the same way perhaps as the $1/f$ noise in C-MOS transistors has been reduced by careful material studies.

11   Concluding remarks and perspectives

The logical thread through this review of superconducting qubits has been the question "What is the best qubit design?". Because some crucial experimental data is still missing, we unfortunately, at present, cannot conclude by giving a definitive answer to this complex optimization problem.

Yet, a lot has already been achieved, and superconducting qubits are becoming serious competitors of trapped ions and atoms. The following properties of quantum circuits have been demonstrated:

a) Coherence quality factors $Q_\varphi = T_\varphi \omega_{01}$ can attain at least $2{\times}10^4$.

b) Readout and reset fidelity can be greater than 95%.

c) All states on the Bloch sphere can be addressed.

d) Spin echo techniques can null out low frequency drift of offset charges.

e) Two qubits can be coupled and RF pulses can implement gate operation.

f) A qubit can be fabricated using only optical lithography techniques.

The major problem we are facing is that these various results have not been obtained at the same time in the same circuit, although succesful design elements in one have often been incorporated into the next generation of others. The complete optimization of the single qubit plus readout has not been achieved yet. However, we have presented in this review the elements of a systematic methodology resolving the various conflicts that are generated by all the different requirements. Our opinion is that, once noise sources are better characterized, an appropriate combination of all the known circuit design strategies for improving coherence, as well as the understanding of optimal tunnel layer growth conditions for lowering the intrinsic noise of Josephson junctions, should lead us to reach the 1-qubit and 2-qubit coherence levels needed for error correction [46]. Along the way, good medium term targets to test overall progress on the simultaneous fronts of qubit coherence, readout and gate coupling are the measurement of Bell 's inequality violation or the implementation of the Deutsch-Josza algorithm, both of which requiring the simultaneous satisfaction of properties a)-e).

Acknowlegements

Appendix

A   Quantum circuit theory

The problem we are addressing in this section is, given a superconducting circuit made up of capacitors, inductors and Josephson junctions, how to systematically write its quantum hamiltonian, the generating function from which the quantum dynamics of the circuit can be obtained. This problem has been considered first

34

by Yurke and Denker[47] in a seminal paper and analyzed in further details by Devoret[48]. We will only summarize here the results needed for this review.

The circuit is given as a set of branches, which can be capacitors, inductors or Josephson tunnel elements, connected at nodes. Several independent paths formed by a succession of branches can be found between nodes. The circuit can therefore contain one or several loops. It is important to note that a circuit has not one hamiltonian but many, each one depending on a particular representation. We are describing here one particular type of representation, which is usually well adapted to circuits containing Josephson junctions. Like in classical circuit theory, a set of independent current and voltages has to be found for a particular representation. We start by associating to each branch b of the circuit, the current i_b flowing through it and the voltage v_b across it (a convention has to be made first on the direction of the branches). Kirchhoff's laws impose relations among branch variables and some of them are redundant. The following procedure is used to eliminate redundant branches: one node of the circuit is first chosen as ground. Then from the ground, a loop-free set of branches called spanning tree is selected. The rule behind the selection of the spanning tree is the following: each node of the circuit must be linked to the ground by one and only one path belonging to the tree. In general, inductors (linear or non-linear) are preferred as branches of the tree but this is not necessary. Once the spanning tree is chosen (note that we still have many possibilities for this tree), we can associate to each node a "node voltage" v_n which is the algebraic sum of the voltages along the branches between ground and the node. The conjugate "node current" i_n is the algebraic sum of all currents flowing to the node through capacitors only. The dynamical variables appearing in the hamiltonian of the circuit are the node fluxes and node charges defined as

$$
\begin{aligned}
\phi_n &= \int_{-\infty}^{t} v\left(t_1\right) dt_1 \\
q_n &= \int_{-\infty}^{t} i\left(t_1\right) dt_1
\end{aligned}
$$

Using Kirchhoff's laws, it is possible to express the flux and the charge of each branch as a linear combination of all the node fluxes and charges, respectively. In this inversion procedure, the total flux through loops imposed by external flux bias sources and polarisation charges of nodes imposed by charge bias sources, appear.

If we now sum the energies of all branches of the circuit expressed in terms of node flux and charges, we will obtain the hamiltonian of the circuit corresponding to the representation associated with the particular spanning tree. In this hamiltonian, capacitor energies behave like kinetic terms while the inductor energies behave as potential terms. The hamiltonian of the LC circuit written in section 2 is an elementary example of this procedure.

Once the hamiltonian is obtained it is easy get its quantum version by replacing all the node fluxes and charges by their quantum operator equivalent.

The flux and charge of a node have a commutator given by $i\hbar$, like the position and momentum of a particle:

$$
\begin{aligned}
\phi &\rightarrow \hat{\phi} \\
q &\rightarrow \hat{q} \\
\left[\hat{\phi}, \hat{q}\right] &= i\hbar
\end{aligned}
$$

One can also show that the flux and charge operators corresponding to a branch share the same commutation relation. Note that for the special case of the Josephson element, the phase $\hat{\theta}$ and Cooper pair number $\hat{N}$, which are its dimensionless electric variables, have the property:

$$
\left[\hat{\theta}, \hat{N}\right] = i
$$

In the so-called charge basis, we have

$$
\begin{aligned}
\hat{N} &= \sum_N N \left|N\right\rangle \left\langle N\right| \\
\cos\hat{\theta} &= \frac{1}{2} \sum_N \left(\left|N\right\rangle \left\langle N+1\right| + \left|N+\right\rangle \left\langle N\right|\right)
\end{aligned}
$$

while in the so-called phase basis, we have

$$
\hat{N} = \left|\theta\right\rangle \frac{\partial}{i\partial} \left\langle \theta\right|
$$

Note that since the Cooper pair number $\hat{N}$ is an operator with integer eigenvalues, its conjugate variable $\hat{\theta}$, has eigenvalues behaving like angles, i.e. they are defined only modulo 2π.

In this review, outside this appendix, we have dropped the hat on operators for simplicity.

B   Eigenenergies and eigenfunctions of the Cooper pair box

From Appendix A, it easy to see that the hamiltonian of the Cooper pair box leads to the Schrodinger equation

$$
\left[E_C \left(\frac{\partial}{i\partial\theta} - N_g\right)^2 - E_J \cos\theta\right] \Psi_k\left(\theta\right) = E_k \Psi_k\left(\theta\right)
$$

The functions $\Psi_k(\theta)\,e^{-iN_g}$ and energies E_k are solutions of the Mathieu equation and can be found with arbitrary precision for all values of the parameters N_g and E_J/E_C[49]. For instance, using the program Mathematica, we find

$$E_k = E_C \mathcal{M}_A \left[k+1-(k+1)\,\mathrm{mod}2 + 2N_g(-1)^k, -2E_J/E_C \right]$$

$$\Psi_k(\theta) = \frac{e^{iN_g\theta}}{\sqrt{2\pi}} \left\{ \mathcal{M}_C \left[\frac{4E_k}{E_C}, \frac{-2E_J}{E_C}, \frac{\theta}{2} \right] + i(-1)^{k+1}\mathcal{M}_S \left[\frac{4E_k}{E_C}, \frac{-2E_J}{E_C}, \frac{\theta}{2} \right] \right\}$$

where $\mathcal{M}_A(r,q) = \texttt{MathieuCharacteristicA[r,q]}$,
$\mathcal{M}_C(a,q,z) = \texttt{MathieuC[a,q,z]}$,
$\mathcal{M}_S(a,q,z) = \texttt{MathieuS[a,q,z]}$.

C Relaxation and decoherence rates for a qubit

C.1 Definition of the rates

We start by introducing the spin eigenreference frame $\hat{z}$, $\hat{x}$ and $\hat{y}$ consisting of the unit vector along the eigenaxis and the associated orthogonal unit vectors ($\hat{x}$ is in the XZ plane). For instance, for the Cooper pair box, we find that $\hat{z} = \cos\alpha\hat{Z} + \sin\alpha\hat{X}$, with $\tan\alpha = 2E_C(N_g - 1/2)/E_J$, while $\hat{x} = -\sin\alpha\hat{Z} + \cos\alpha\hat{X}$.

Starting with $\overrightarrow{S}$ pointing along $\hat{x}$ at time $t=0$, the dynamics of the Bloch vector in absence of relaxation or decoherence is

$$\overrightarrow{S}_0(t) = \cos(\omega_{01})\,\hat{x} + \sin(\omega_{01})\,\hat{y}$$

In presence of relaxation and decoherence, the Bloch vector will deviate from $\overrightarrow{S}_0(t)$ and will reach eventually the equilibrium value $S_z^{eq}\hat{z}$, where $S_z^{eq} = \tanh(\hbar\omega_{01}/2k_BT)$.

We define the relaxation and decoherence rates as

$$\Gamma_1 = \lim_{t\to\infty} \frac{\ln\langle S_z(t) - S_z^{eq}\rangle}{t}$$

$$\Gamma_\phi = \lim_{t\to\infty} \frac{\ln\left[\frac{\langle \overrightarrow{S}(t).\overrightarrow{S}_0(t)\rangle}{\left|\overrightarrow{S}(t) - S_z^{eq}\hat{z}\right|}\right]}{t}$$

Note that these rates have both a useful and rigorous meaning only if the evolution of the components of the average Bloch vector follows, after a negligibly short settling time, an exponential decay. The Γ_1 and Γ_ϕ rates are related to the NMR spin relaxation times T_1 and T_2 [50] by

$$T_1 = \Gamma_1^{-1}$$
$$T_2 = (\Gamma_\phi + \Gamma_1/2)^{-1}$$

The T_2 time can be seen as the net decay time of quantum information, including the influence of both relaxation and dephasing processes. In our discussion of superconducting qubits, we must separate the contribution of the two types of processes since their physical origin is in general very different and cannot rely on the T_2 time alone.

C.2   Expressions for the rates

The relaxation process can be seen as resulting from unwanted transitions between the two eigenstate of the qubit induced by fluctuations in the effective fields along the x and y axes. Introducing the power spectral density of this field, one can demonstrate from Fermi's Golden Rule that, for perturbative fluctuations,

$$\Gamma_1 = \frac{S_x(\omega_{01}) + S_y(\omega_{01})}{\hbar^2}$$

Taking the case of the Cooper pair box as an example, we find that $S_y(\omega_{01}) = 0$ and that

$$S_x(\omega) = \int_{-\infty}^{+\infty} dt e^{i\omega t} \langle A(t) A(0) \rangle + \langle B(t) B(0) \rangle$$

where

$$A(t) = \frac{\Delta E_J(t) E_{el}}{2\sqrt{E_J^2 + E_{el}^2}}$$
$$B(t) = \frac{E_J \Delta E_{el}(t)}{2\sqrt{E_J^2 + E_{el}^2}}$$
$$E_{el} = 2E_C(N_g - 1/2)$$

Since the fluctuations $\Delta E_{el}(t)$ can be related to the impedance of the environment of the box[19, 21, 51], an order of magnitude estimate of the relaxation rate can be performed, and is in rough agreement with observations [52, 22].

The decoherence process, on the other hand, is induced by fluctuations in the effective field along the eigenaxis z. If these fluctuations are Gaussian, with a white noise spectral density up to frequencies of order several Γ_ϕ (which is often not the case because of the presence of 1/f noise) we have

$$\Gamma_\phi = \frac{S_z\left(\omega \simeq 0\right)}{\hbar^2}$$

In presence of a low frequency noise with an 1/f behavior, the formula is more complicated[53]. If the environment producing the low frequency noise consists of many degrees of freedom, each of which is very weakly coupled to the qubit, then one is in presence of classical dephasing which, if slow enough, can in principle be fought using echo techniques. If, on the other hand, only a few degrees of freedom like magnetic spins or glassy two-level systems are dominating the low frequency dynamics, dephasing is quantum and not correctable, unless the transition frequencies of these few perturbing degrees of freedom is itself very stable.

References

[1] M. A. Nielsen and I. L. Chuang, *Quantum Computation and Quantum Information* (Cambridge, 2000).

[2] M. Tinkham, *Introduction to Superconductivity* (Krieger, Malabar, 1985).

[3] J. M. Martinis, M. H. Devoret, J. Clarke, Phys. Rev. Lett. 55, 1543-1546 (1985); M. H. Devoret, J. M. Martinis, J. Clarke, Phys. Rev. Lett. 55, 1908-1911 (1985); J. M. Martinis, M. H. Devoret and J. Clarke, Phys. Rev. 35, 4682 (1987).

[4] J. M. Martinis and M. Nahum, Phys Rev. B 48, 18316-19 (1993).

[5] B. D. Josephson, in *Superconductivity*, R. D. Parks, ed. (Marcel Dekker, New York, 1969).

[6] K. K. Likharev, *Dynamics of Josephson Junctions and Circuits* (Gordon and Breach, New York, 1986)

[7] I. Giaever, Phys. Rev. Lett. 5, 147, 464 (1960)

[8] A. O. Caldeira and A. J. Leggett, Ann. Phys. (NY) 149, 347-456 (1983); A. J. Leggett, J. Phys. CM 14, R415-451 (2002).

[9] D. P. DiVincenzo, arXiv:quant-ph/0002077,

[10] R. P. Feynman, *Lectures on Physics* (Addison-Wesley, Reading, 1964) Vol. 2, Chap. 23.

[11] D. C. Mattis and J. Bardeen, Phys. Rev. 111, 412 (1958)

[12] P. G. de Gennes, *Superconductivity of Metals and Alloys* (Benjamin, New York, 1966)

[13] J. M. Raimond, M. Brune and S. Haroche, Rev. Mod. Phys. 73, 565 (2001).

[14] J. M. Martinis and K. Osborne, in *Quantum Information and Entanglement*, Eds. J.M. Raimond, D. Esteve and J. Dalibard, Les Houches Summer School Series, arXiv:cond-mat/0402430

[15] J. Clarke, Proc. IEEE 77, 1208 (1989)

[16] D. J. Van Harlingen, B. L. T. Plourde, T. L. Robertson, P. A. Reichardt, and John Clarke, Phys. Rev. B 70, 064517 (2004)

[17] R. W. Simmonds, K. M. Lang, D. A. Hite, S. Nam, D. P. Pappas, and J. M. Martinis, Phys. Rev. Lett. 93, 077003 (2004)

[18] M. Büttiker, Phys. Rev. B 36, 3548 (1987).

[19] V. Bouchiat, D. Vion, P. Joyez, D. Esteve, M. H. Devoret, Physica Scripta T76 (1998) p.165-70.

[20] Y. Nakamura , Yu. A Pashkin, and J. S. Tsai, Nature 398, 786 (1999).

[21] Yu. Makhlin, G. Schön, and A. Shnirman, Rev. Mod. Phys. 73, 357-400 (2001).

[22] D. Vion, A. Aassime, A. Cottet, P. Joyez, H. Pothier, C. Urbina, D. Esteve, and M.H. Devoret, Science 296 (2002), p. 286-9.

[23] A. Barone and G. Paternò, *Physics and Applications of the Josephson Effect* (Wiley, New York, 1992)

[24] S. Han, R. Rouse and J. E. Lukens, Phys. Rev. Lett. 84, 1300 (2000); J. R. Friedman, V. Patel, W. Chen, S. K. Tolpygo and J. E. Lukens, Nature 406, 43 (2000).

[25] J. E. Mooij, T. P. Orlando, L. Levitov, Lin Tian, C. H. van der Wal and S. Lloyd, Science 285, 1036 (1999); C. H. van der Wal, A. C. J. ter Haar, F. K. Wilhem, R. N. Schouten, C. Harmans, T. P. Orlando, S. Loyd and J. E. Mooij, Science 290, 773 (2000).

[26] J. M. Martinis, S. Nam, J. Aumentado, and C. Urbina, Phys. Rev. Lett. 89, 117901 (2002)

[27] M. Steffen, J. Martinis and I. L. Chuang, Phys. Rev. B 68, 224518 (2003).

[28] M. H. Devoret and R. J. Schoelkopf, Nature 406, 1039 (2002).

[29] A. N. Korotkov, D. V. Averin, Phys. Rev. B 64, 165310 (2001)

[30] A. Cottet, D. Vion, A. Aassime, P. Joyez, D. Esteve, and M. H. Devoret, Physica C 367, 197 (2002)

[31] I. Siddiqi, R. Vijay, F. Pierre, C. M. Wilson, M. Metcalfe, C. Rigetti, L. Frunzio and M. Devoret, submitted to Phys. Rev. Lett., arXiv:cond-mat/0312623.

[32] D. Vion, A. Aassime, A. Cottet, P. Joyez, H. Pothier, C. Urbina, D. Esteve, and M. H. Devoret, Fortschritte der Physik 51, 462 (2003)

[33] I. Chiorescu, Y. Nakamura, C. J. P. M. Harmans, and J. E. Mooij, Science 299, 1869 (2003).

[34] A. Blais, Ren-Shou Huang, A. Wallraff, S. M. Girvin, R. J. Schoelkopf, Phys. Rev. A 69, 062320 (2004)

[35] A. Lupascu, C. J. M. Verwijs, R. N. Schouten, C. J. P. M. Harmans, J. E. Mooij, arXiv:cond-mat/0311510.

[36] A. Wallraff, D. I. Schuster, A. Blais, L. Frunzio, R.-S. Huang, J. Majer, S. Kumar, S. M. Girvin and R. J. Schoelkopf, Nature (London) 431, 162 (2004).

[37] D. I. Schuster, A. Wallraff, A. Blais, L. Frunzio, R.-S. Huang, J. Majer, S. M. Girvin and R. J. Schoelkopf, submitted to Phys. Rev. Lett. arXiv:cond-mat/0408367.

[38] D.V. Averin, C. Bruder, Phys. Rev. Lett. 91, 057003 (2003).

[39] A. Blais, A. Maassen van den Brink, A. M. Zagoskin, Phys. Rev. Lett. 90, 127901 (2003)

[40] Pashkin Yu. A., Yamamoto T., Astafiev O., Nakamura Y., Averin D. V., and Tsai J. S., Nature 421, 823-826 (2003).

[41] J. B. Majer, *Superconducting Quantum Circuits,* Ph. D. Thesis, TU Delft, (2002); J. B. Majer, F. G. Paauw, A. C. J. ter Haar, C. P. J. Harmans, J. E. Mooij, arXiv:cond-mat/0308192.

[42] A. J. Berkley, H. Xu, R. C. Ramos, M. A. Gubrud, F. W. Strauch, P. R. Johnson, J. R. Anderson, A. J. Dragt, C. J. Lobb, F. C. Wellstood, Science 300, 1548 (2003).

[43] C. Rigetti and M. Devoret, unpublished

[44] Nakamura Y., Pashkin Yu. A., and Tsai J. S., Phys. Rev. Lett. 88, 047901 (2002).

[45] D. Vion, A. Aassime, A. Cottet, P. Joyez, H. Pothier, C. Urbina, D. Esteve, and M. H. Devoret, Forts. der Physik 51, 462 (2003); E. Collin, G. Ithier, A. Aassime, P. Joyez, D. Vion and D. Esteve, submitted to Phys. Rev. Lett., arXiv:cond-mat/0404503.

[46] J. Preskill, J. Proc. R. Soc. London Ser. A454, 385 (1998).

[47] B. Yurke and J. S. Denker, Phys. Rev. A 29, 1419 (1984).

[48] M. H. Devoret in *"Quantum Fluctuations"*, S. Reynaud, E. Giacobino, J. Zinn-Justin, eds. (Elsevier, Amsterdam, 1996) p. 351

[49] A. Cottet, *Implementation of a quantum bit in a superconducting circuit,* PhD Thesis, Université Paris 6, 2002

[50] A. Abragam, Principles of Nuclear Magnetic Resonance (Oxford University Press, Oxford, 1985).

[51] R. J. Schoelkopf, A. A. Clerk, S. M. Girvin, K. W. Lehnert, M. H. Devoret. arXiv:cond-mat/0210247.

[52] K. W. Lehnert, K. Bladh, L. F. Spietz, D. Gunnarsson, D. I. Schuster, P. Delsing, and R. J. Schoelkopf, Phys. Rev. Lett. 90, 027002 (2002).

[53] J. M. Martinis, S. Nam, J. Aumentado, K. M. Lang, and C. Urbina, Phys. Rev. B 67, 462 (2003).